Hindawi
Advances in Civil Engineering
Volume 2022, Article ID 9998019, 13 pages
https://doi.org/10.1155/2022/9998019

Research Article

Time-Frequency Characteristics of Ground Motion and Seismic Response Analysis of Typical Structures in the Yangbi Earthquake in Yunnan Province

Qin Xu,[1] Shaofeng Chai,[2,3] Shihu Zhou,[1] Liqun Bao,[1] and Quan Li[1]

[1]*Lanzhou Institute of Technology, Lanzhou 730050, China*
[2]*Key Laboratory of Earthquake Engineering and Engineering Vibration of China Earthquake Agency, Institute of Engineering Mechanics, China Earthquake Agency, Harbin 150080, Heilongjiang, China*
[3]*Key Laboratory of Loess Earthquake Engineering of China Earthquake Administration & Gansu Province, Lanzhou 730000, Gansu, China*

Correspondence should be addressed to Shaofeng Chai; chaishaofeng520@163.com

Received 15 March 2022; Accepted 27 May 2022; Published 20 July 2022

Academic Editor: Ping Xiang

The ground motion records obtained by the CDSMON during the Ms6.4 earthquake in Yangbi, Yunnan Province, on May 21, 2021, were subjected to routine processing such as baseline correction and filtering. The nonstationary time-frequency characteristics of ground motion signals were analysed by the wavelet transform, and the acceleration response spectrum characteristics of typical stations under different epicentral distances, magnitudes, and site conditions were analysed. Finite element software was used to establish a model to analyse the seismic response of a typical three-span continuous beam bridge. The maximum peak ground acceleration (PGA) of this earthquake (720.29 gal) was obtained from 53YBX in the NS direction at the epicentral distance of 8.6 km. The energy at station 53YBX was mainly concentrated in 0–15 Hz range, and the low-frequency component energy caused great damage to buildings with natural frequencies in this frequency band. The Sa value near the origin of the earthquake is relatively large, as the distance from the epicentre increases, the predominant period of Sa also gradually increases, and the high-frequency component diminishes. With the increase in earthquake magnitude, the Sa peak increased, and the long-period component became more obvious. The soil station had more obvious long-period components than the bedrock station, which is consistent with the amplification result of the response spectrum of overburden thickness to surface acceleration. The earthquake had little influence on the pier displacement of the three-span continuous beam bridge with a fundamental period of 0.77 s but had a great influence on the bending moment at the bottom of the piers.

1. Introduction

According to the measurement of the China Earthquake Networks Center, at 21 : 48 on May 21, 2021, an Ms6.4 earthquake occurred in Yangbi County, Dali Prefecture, Yunnan Province. The epicentre was located at 25.67°N and 99.87°E, and the focal depth was 8 km. The earthquake belongs to a typical foreshock-mainshock-aftershock event. More than 350 seismicities occurred before the mainshock, including five earthquakes with a magnitude of Ms4.0 or above. The largest foreshock was the Ms5.6 earthquake at 21 : 21 on May 21, 2021, with the epicentre at 25.67°N and 99.87°E, a focal depth of 10 km, and a distance from the Ms6.4 mainshock of 6 km. After the mainshock, the Yunnan regional seismic network recorded rich sequences of aftershocks. As of May 26, 2021, 2426 aftershocks above magnitude 0 have been recorded. The largest aftershock was the Ms5.2 earthquake at 22 : 31 on May 21, 2021, with the epicentre at 25.59 N and 99.97°E) and a focal depth of 8 km [1]. The seismogenic fault of this earthquake was a NW-trending secondary fault on the west side of the Weixi-Qiaohou fault, which is dominated by dextral strike-slip motion [2, 3]. On May 25, the Yunnan Provincial Seismological Bureau issued the intensity map of the Ms6.4 Yangbi earthquake in Yunnan Province, which shows that the maximum intensity of this earthquake was VIII and that

the area of intensity VI and above was approximately 6600 km^2, involving 6 counties and cities of Dali Prefecture.

The China Digital Strong Motion Observation Network (CDSMON) captured abundant records of strong ground motions after the earthquake. Chen and Li [4] conducted conventional processing such as filtering on the ground motion records, analysed the attenuation patterns and duration characteristics of the ground motion amplitude, and compared the recorded acceleration response spectra of stations with different epicentral distances. Tian et al. [5] compared and analysed the acceleration response spectra of 6 stations with the nearest epicentral distances and largest amplitudes. The aforementioned studies analysed the frequency domain characteristics of ground motion mainly based on acceleration response spectra.

Ground motion records belong to nonstationary time-varying signals, and their energy and frequency will change greatly with time [6]. Conventional signal processing methods cannot well reflect the time dependence of frequency components, while the wavelet transform and wavelet packet transform are time-frequency analysis methods suitable for nonstationary signals [7, 8]. Therefore, based on the conventional processing of ground motion records such as baseline correction and filtering, the wavelet and wavelet packet transforms are introduced to analyse their time-frequency characteristics. In the analysis of acceleration response spectra, in addition to the comparative analysis of the response spectrum characteristics of different epicentral distances, the response spectrum characteristics of different earthquake magnitudes at the same stations and the response spectrum characteristics of stations with similar epicentral distances but different site conditions, such as soil and bedrock, are comparatively analysed. In addition, a typical finite element model of a continuous beam bridge is established to analyse the stress of the model under the Ms6.4 earthquake in Yangbi, Yunnan Province. This study further explores the influence pattern of the nonstationary ground motion signal on the time-frequency characteristics of the structure, which has more in-depth research value and significance.

2. Collection and Processing of Strong Motion Records

Baseline correction, filtering, and other conventional data processing [9] were conducted on the uncorrected acceleration records. (1) The average value of acceleration recorded 20 s before the time of recording the original acceleration was calculated and subtracted from the recorded original acceleration, and then, the recorded zero drift was adjusted. (2) The acceleration records after zero-line adjustment were subjected to bidirectional high-pass filtering through a digital filter (4th-order Butterworth) in the cutoff frequency range of 0.01–100 Hz selected according to the Nyquist sampling rate. (3) The corrected acceleration records were filtered according to the Interim Code for computing the instrumental seismic intensity in the cutoff frequency range of 0.1–10 Hz, and the instrumental seismic intensities were computed. The basic information and related parameters of typical strong earthquake records corresponding to the strong motion stations of the Ms6.4 earthquake are shown in Table 1. The maximum peak ground acceleration (PGA) of this earthquake (720.29 gal) was obtained from 53YBX (Yangbi Station that is 8.6 km far from the epicentral distance) in the NS direction. The records obtained in this earthquake were mostly far-field records and rarely near-field records.

3. Wavelet and Wavelet Packet Analysis

The wavelet transform and wavelet packet transform are tools of signal analysis and time-frequency analysis methods suitable for nonstationary signals [10]. The wavelet transform inherits and develops the idea of localization in the short-time Fourier transform (STFT) [11], which makes up for the shortcomings that the window width cannot be applied to any frequency and provides a time-frequency window that changes with frequency [12]. As a generalization and extension of the wavelet transform, the wavelet packet transform can provide a more refined signal analysis method [13]. Compared with the conventional Fourier transform and wavelet transform, the advantage of the wavelet packet transform is that it divides the time-frequency plane more finely and improves the resolution of the high-frequency component of the signal [14].

3.1. Wavelet Transform Analysis. Considering that the waveform of a Daubechies wavelet is very similar to that of a ground motion velocity pulse in terms of high compactness, smoothness, and approximate symmetry [15], Daubechies 8 was used as the wavelet basis in this study. The time-frequency analysis of the ground motion signal of the Ms6.4 earthquake is carried out using a one-dimensional continuous wavelet transform [16]. The strong motion records in three directions (EW, NS, and UD) obtained at station 53YBX were selected for wavelet analysis. The analysis results are shown in Figure 1. In the frequency domain, the overall low-frequency signal energy is strong, the high-frequency signal energy is weak, and the energy in three directions is mainly concentrated in the 0–15 Hz range. In the time domain, there are two energy peaks in the EW and NS directions at 32–34 s and 36–38 s and one energy peak in the UD direction at 36–38 s. In general, the energy peak in the UD direction has a larger width and lower wavelet coefficients than those in the EW and NS directions.

3.2. Wavelet Packet Transform Analysis. In this study, Daubechies 8 was still used as the wavelet base for wavelet packet decomposition. The sampling rate of the strong seismograph was 200 Hz. Considering the requirements of resolution and refinement, five-layer wavelet packet decomposition was selected, so the minimum frequency bandwidth was 1.5625 Hz. In addition, the sequence number sorting disorder occurs in wavelet packet decomposition. The MATLAB program was written using the method proposed in a past study [17] to realize the function of frequency sorting with a node sequence number. The frequency band energy ratio was intercepted within 0.1, and Figures 2–4 show the

Table 1: Typical strong motion records and some related parameters of the Ms 6.4 earthquake at epicentral distances of less than 200 km.

Station code	Station type	Epicentral distance (km)	PGA/cm/s/s			PGV/cm/s			Instrumental intensity
			EW	NS	UD	EW	NS	UD	
53YBX	Soil	8.6	−379.88	−720.29	−448.36	30.26	−29.4	−7.32	8.9
53DLY	Soil	31.3	−116.41	−108.25	−91.02	−8.45	11.48	2.24	6.95
53YPX	Soil	40.0	−44.94	−65.16	—	3.43	−7.39	—	—
53BTH	Rock	67.7	7.36	6.97	−6.05	0.53	−0.74	0.64	3.29
53BCJ	Soil	72.6	−22.5	−24.3	−18	−2.7	2.47	1.37	5.12
53LKT	Rock	103.5	−10.15	9.66	−12.84	−0.53	−0.48	−0.32	3.51
53SDX	Soil	124.0	19.06	−27.34	9.61	3.25	−4.49	0.78	5.39
53YRH	Soil	145.1	−6.2	−4.41	3.12	−0.64	0.57	0.24	3.09
53LLP	Soil	160.0	−2.41	−3.17	−1.56	−0.34	0.23	−0.11	2.23
51PZF	Soil	184.6	−2.39	2.74	−1.11	0.33	−0.34	0.18	2.17
53MST	Soil	190.2	−5.1	4.8	2.49	0.48	1.02	−0.26	3.2
51PZT	Soil	198.9	−4.95	4	−1.2	−0.26	0.26	0.08	2.41

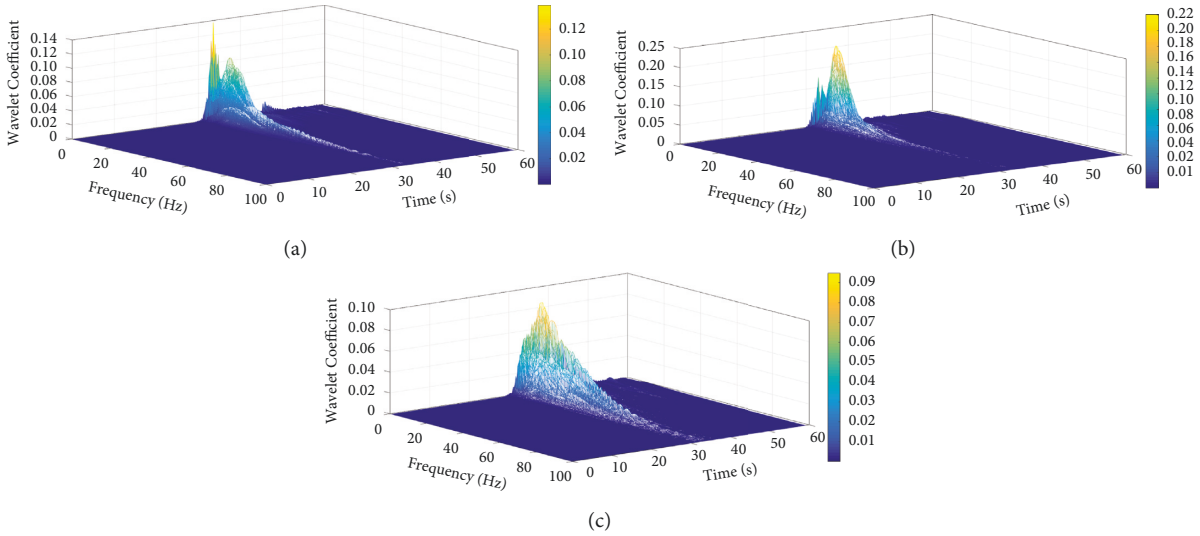

Figure 1: Wavelet time-frequency analysis of earthquake records at 53YBX: (a) east-west; (b) north-south; and (c) vertical.

distribution of the seismic energy spectrum of the Ms6.4 earthquake at stations with different epicentral distances.

The energy in the EW and NS directions at 53YBX (8.6 km from the epicentre), which was closest to the epicentre, is mainly distributed in the first 8 modes (0–12.5 Hz), the energy in the UD direction is more widely distributed in the first 13 modes (0–20.3 Hz), the energy in the EW direction peaks in the 0–1.6 Hz range, and the energy in the NS direction peaks in the 4.7–6.2 Hz range. There is no sudden increase in energy in the frequency band in the UD direction, and the width of the dominant energy band accounts for a large proportion. For 53DLY (31.3 km from the epicentre), the energy in the EW and NS directions is mainly distributed in the first 10 modes (0–15.6 Hz), the energy in the UD direction is distributed in the first 11 modes (0–17.2 Hz), the energy in the EW and NS direction peaks in the 0–1.6 Hz range, and the energy in the UD direction peaks in the 9.4–10.9 Hz range. For 53BCJ (72.6 km from the epicentre), the energy in the EW and NS directions is mainly distributed in the first 3 modes (0–4.7 Hz), the energy in the UD direction is distributed in the first 5 modes (0–7.8 Hz), and the energy peaks in the 0–1.6 Hz range is distributed in all three directions. It is found that the width of dominant energy band at stations with different distances from the epicentre of the same earthquake is greater in the UD direction than in the EW and NS directions. With the increase in epicentral distance, the width of the characteristic energy frequency band becomes narrower, the dominant energy is more concentrated in low-frequency bands, and the high-frequency energy decreases.

4. Characteristics of the Acceleration Response Spectra

The acceleration response spectrum is an important basis and method for engineering seismic design. Calculating and analysing the acceleration response spectra are helpful to understand the frequency-domain characteristics of strong earthquake acceleration near the epicentre and directly show the maximum response of structures with different natural periods to earthquakes [18].

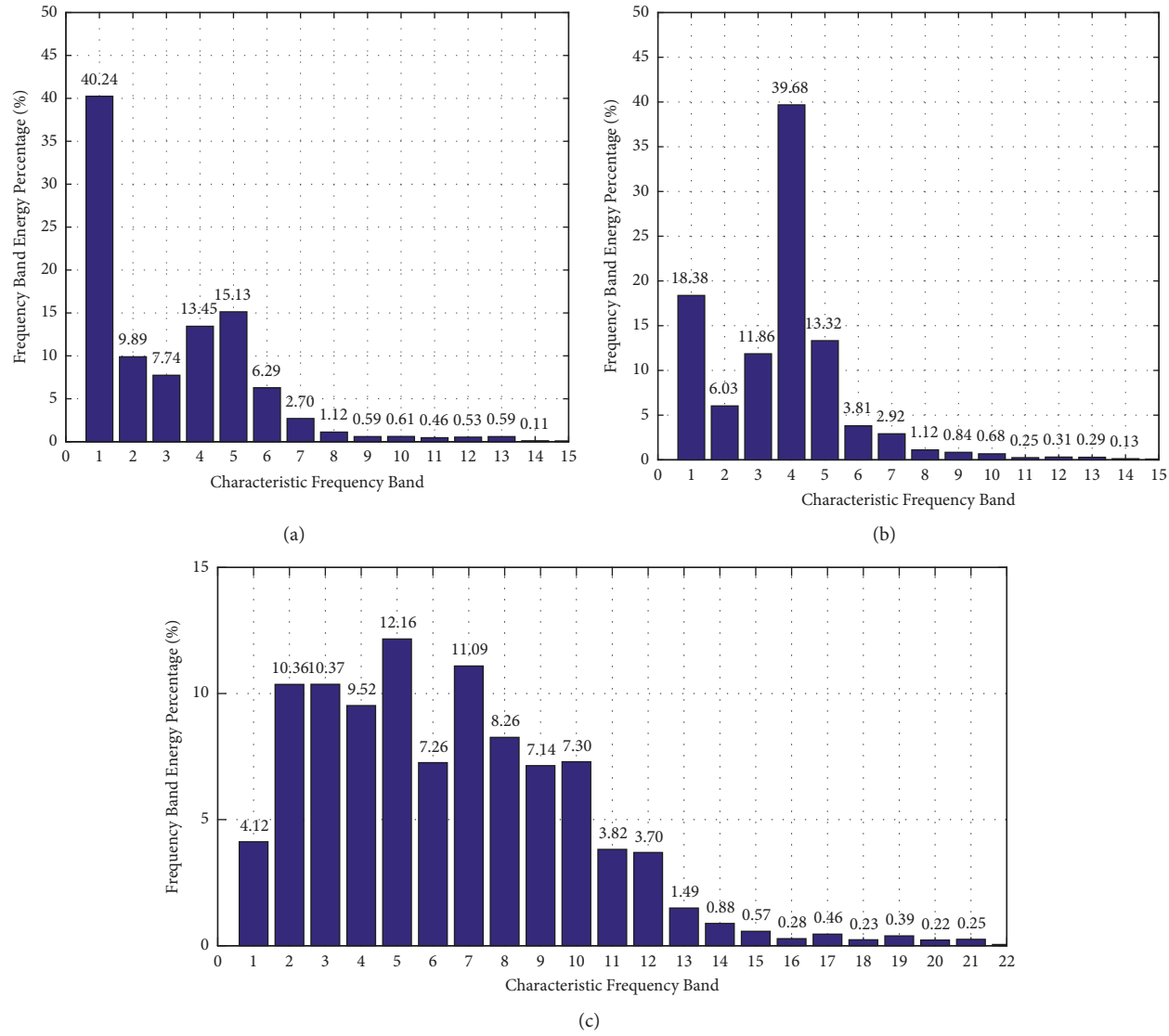

Figure 2: Energy probability distribution of earthquake records at 53YBX (8.6 km from the epicentre): (a) east-west; (b) north-south; (c) and vertical.

4.1. Acceleration Response Spectra of Stations at Different Epicentral Distances. Acceleration response spectra (Sa) of three soil stations (53YBX, 53DLY, and 53BCJ) with different distances from the epicentre of the Ms6.4 earthquake were selected and compared with the seismic design response spectra of the areas where the stations are located (Code for Seismic Design of Buildings (GB 50011–2010)). Station 53YBX is located in Yangbi Yi Autonomous County. For station 53YBX, the seismic fortification intensity is VIII, the design basic seismic acceleration is 0.20 (m/s^2), and the design ground motion group is the third group. The seismic fortification intensity for stations 53DLY and 5BCJ is VIII. As can be seen from Figure 5, there is similarity between the Sa spectra in the three directions of 53YBX (EW, NS, and UD), the predominant period of which is around 0.04–0.09 s. The Sa value in the directions of EW and NS is higher compared with the design spectrum of intensity VIII rare earthquake within 0.1 s. When the period is smaller than 1.2 s, the Sa is higher than the design spectrum of intensity VIII fortification earthquake; in the UD direction, the Sa is higher than the design spectrum of intensity VIII rare earthquake within 0.2 s, and after 3 s, the Sa attenuates to near 0 g. The 53DLY three direction predominant periods of Sa are approximately 0.05–1.1 s, and the Sa is lower than the design spectrum of intensity VIII rare earthquake. When the period is smaller than 1.2 s, the Sa in the EW and NS directions is higher than the design spectrum of intensity VIII frequent earthquake, and in the UD direction, the Sa is higher than the code design spectrum of intensity VIII frequent earthquake within 0.1 s. The Sa in the three directions at station 53BCJ is lower than the design spectrum of intensity VIII frequent earthquake, and the predominant period of Sa is approximately 0.15–1.5 s. The comparison shows that the Sa value near the origin of the earthquake is relatively large. As the distance from the epicentre increases, the predominant period of Sa is also gradually increasing,

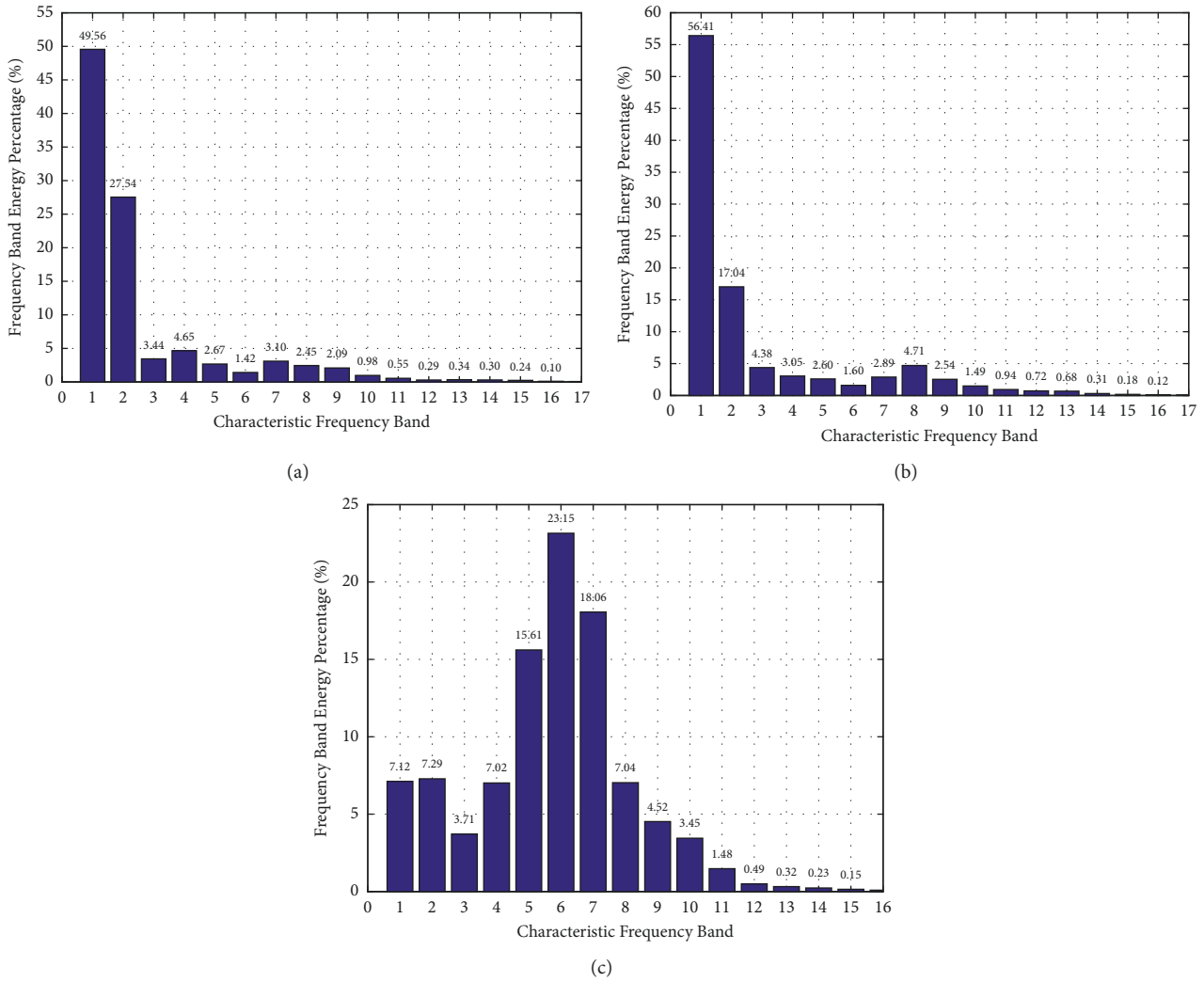

Figure 3: Energy probability distribution of earthquake records at 53DLY (31.3 km from the epicentre): (a) east-west; (b) north-south; and (c) vertical.

the high-frequency component diminishes, and the Sa spectrum shifts to the long period on the whole, which is attributed to the attenuation of the ground motion through the propagation medium. Consequently, the maximum response of the structure is reduced as well.

4.2. Acceleration Response Spectra of Different Earthquake Magnitudes at the Same Station. Three earthquakes (Ms6.4, Ms5.6, and Ms5.2) at the 53YBX station were selected, and their Sa was comparatively analysed (Figure 6). The Sa values of Ms6.4 in three directions within 0.09 s are higher relative to the design spectrum of intensity VIII rare earthquake, while those of Ms5.6 in the directions of EW and NS within 0.1 s are higher compared with the design spectrum of VII rare earthquake, the Sa values in the direction of UD is lower than the design spectrum of intensity VIII rare earthquakes and higher than the design spectrum of intensity VII rare earthquakes with this period and those of Ms5.2 within 0.09 s are higher in comparison with the design spectrum of intensity VIII rare earthquake in the direction of NS. As revealed by the comparison, the Sa spectra of the three earthquakes are consistent in the same direction, and the Sa values in the direction of NS at the same station with different magnitudes of earthquake are greater than in the directions of EW and UD. With an increase in magnitude of the earthquake, the Sa peak value rises and the long-period component becomes more significant.

4.3. Acceleration Response Spectra of Soil and Bedrock Stations with Similar Epicentral Distances. A soil station 53BCJ (epicentral distance is 72.6 km) and a bedrock station 53BTH (epicentral distance is 67.7 km) with similar distances from the epicentre of the same Ms6.4 earthquake were selected. According to the intensity values of the two stations (Table 1), the instrument intensity of the two stations reaches 3.29 and 5.12, respectively. Therefore, the intensity VI frequent and fortification seismic design spectrum is adopted for comparison. As shown in Figure 7, the Sa tridirectional value curve of 53BCJ is lower compared with the intensity VI fortification seismic design spectrum, with the

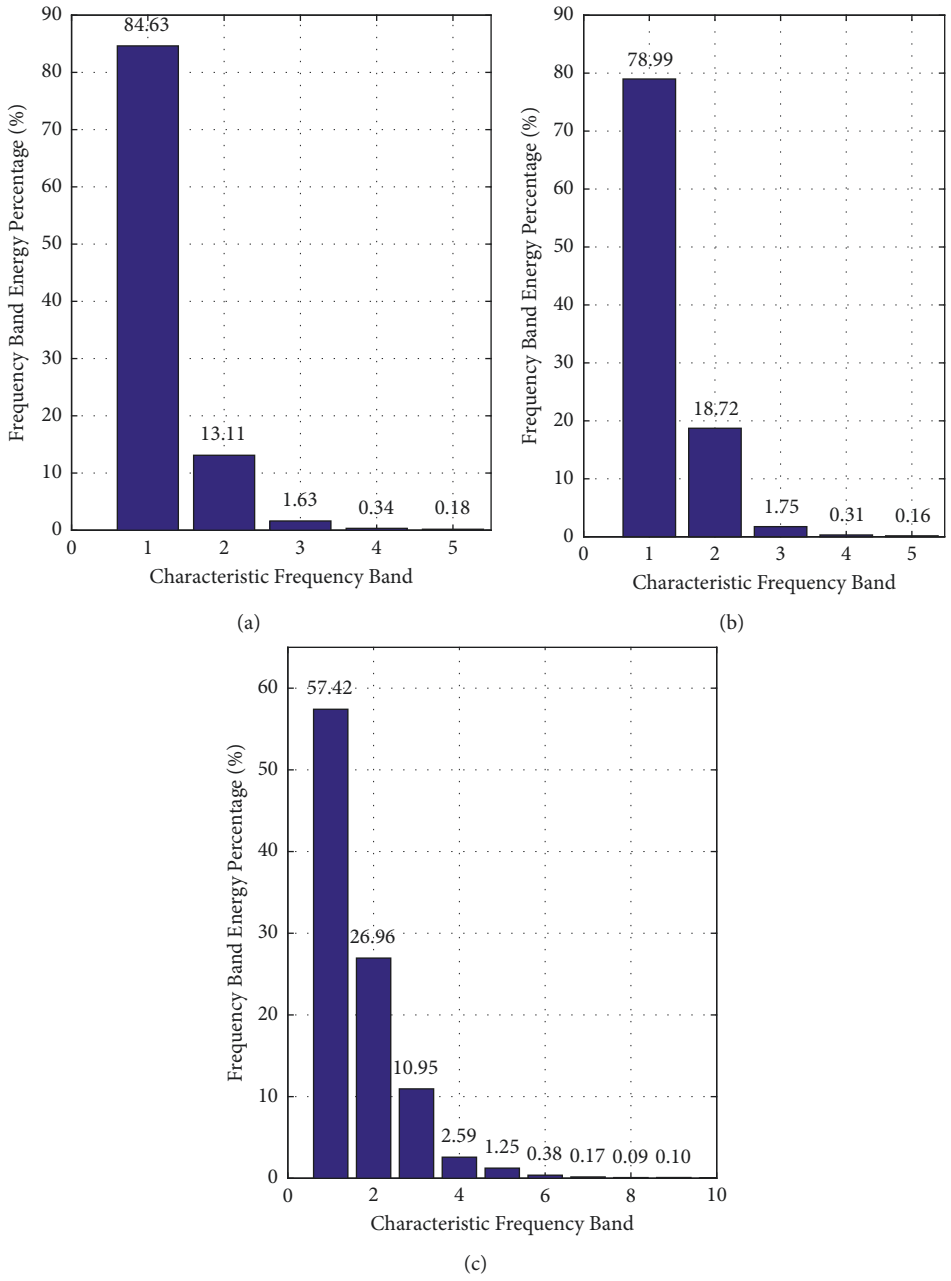

Figure 4: Energy probability distribution of earthquake records at 53BCJ (72.6 km from the epicentre): (a) east-west; (b) north-south; and (c) vertical.

values after 0.2 s in the directions of NS and EW reaching a level that is higher than the intensity VI frequent seismic design spectrum, and the Sa tri-directional values curve of 53BTH is lower compared with the intensity VI seismic design spectrum. According to the comparison, the soil station (53BCJ) has a high peak Sa value and long-cycle component relative to the bedrock station (53BTH), the process of Sa attenuation is slowed, and the overall response spectrum curve shifts to the right. The analysis reveals that site conditions tend to have a significant impact on ground motion and that soil field causes a more evident amplification effect on the acceleration response of ground surface than bedrock. Such amplification is not confined to being manifested in the long-cycle part. Instead, the Sa amplitude of the short-cycle part also increases, which exerts a widespread influence on buildings. The specific amplification factor is related to the thickness of soil overburden [19–21], which is worthy of further study.

5. Seismic Response Analysis of Typical Structures

As the lifeline project of urban construction, the seismic safety of road and bridge structures is of great significance to ensure the normal operation of social, political, and economic life, as well as post-earthquake rescue and reconstruction [22]. In this section, the finite element model of a typical three-span reinforced concrete continuous beam

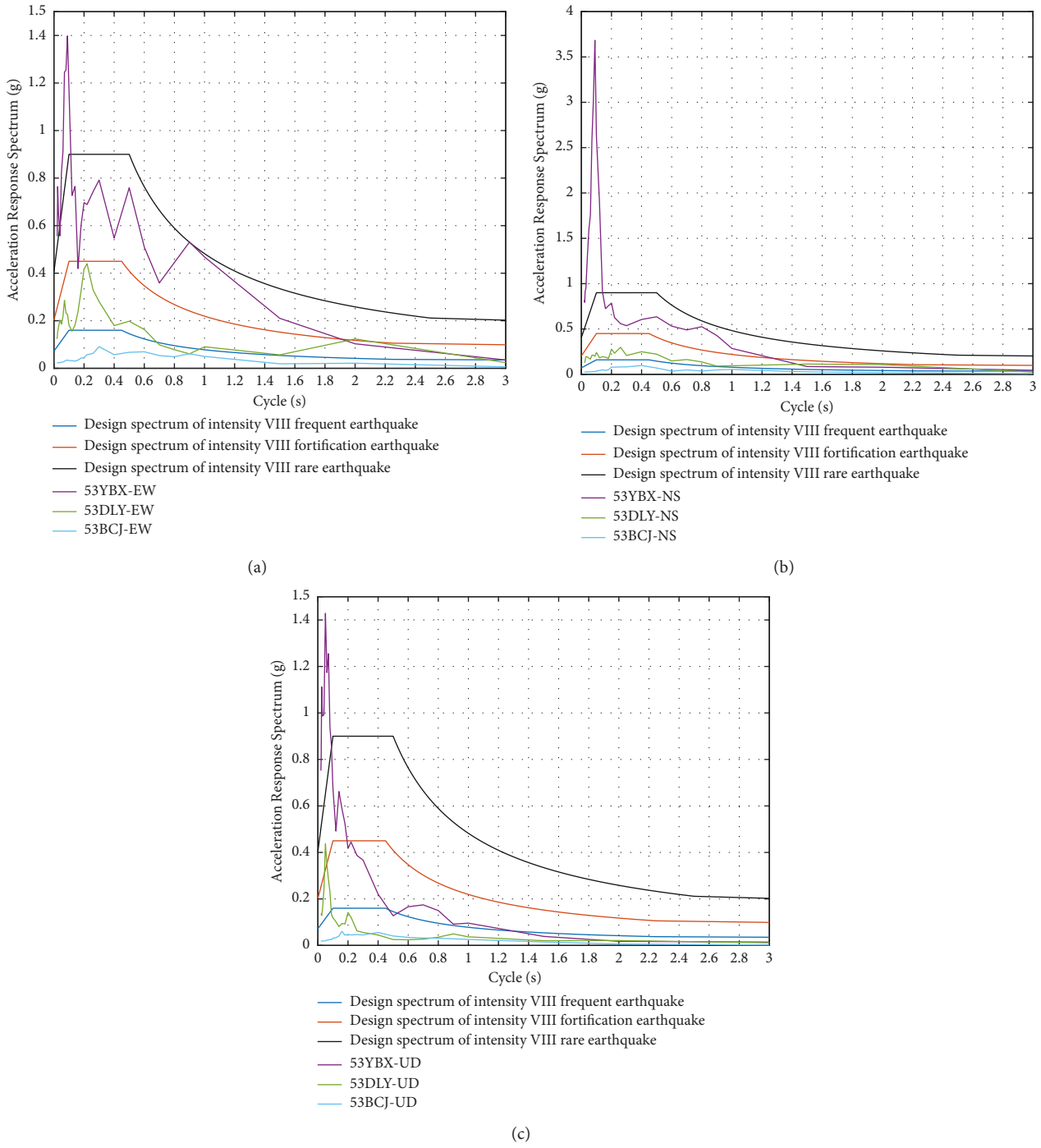

Figure 5: Comparison of acceleration response spectra (Sa) and code design spectra among stations with different epicentral distances: (a) east-west; (b) north-south; and (c) vertical. Note: all acceleration response spectra involved in this section are acceleration response spectra (Sa) with a damping ratio of 5%.

bridge is established to simulate the stress on the bridge under an earthquake, analyse the influence of the parameters of the bridge in the seismic response, and lay a foundation for future seismic research [23].

5.1. Project Overview. A continuous girder bridge is characterized by large structural stiffness, small deformation, few expansion joints, and a smooth and comfortable surface for driving, so it is widely used in the development of modern bridges. In this study, a three-span (40 + 70 + 40) m continuous beam bridge was selected as the model [24]. The bridge elevation is shown in Figure 8. The bridge superstructure is a reinforced concrete continuous box girder, and the substructure consists of rectangular gravity piers [25]. The size of each pier is 8 m × 3.5 m × 5.0 m. The diameter of

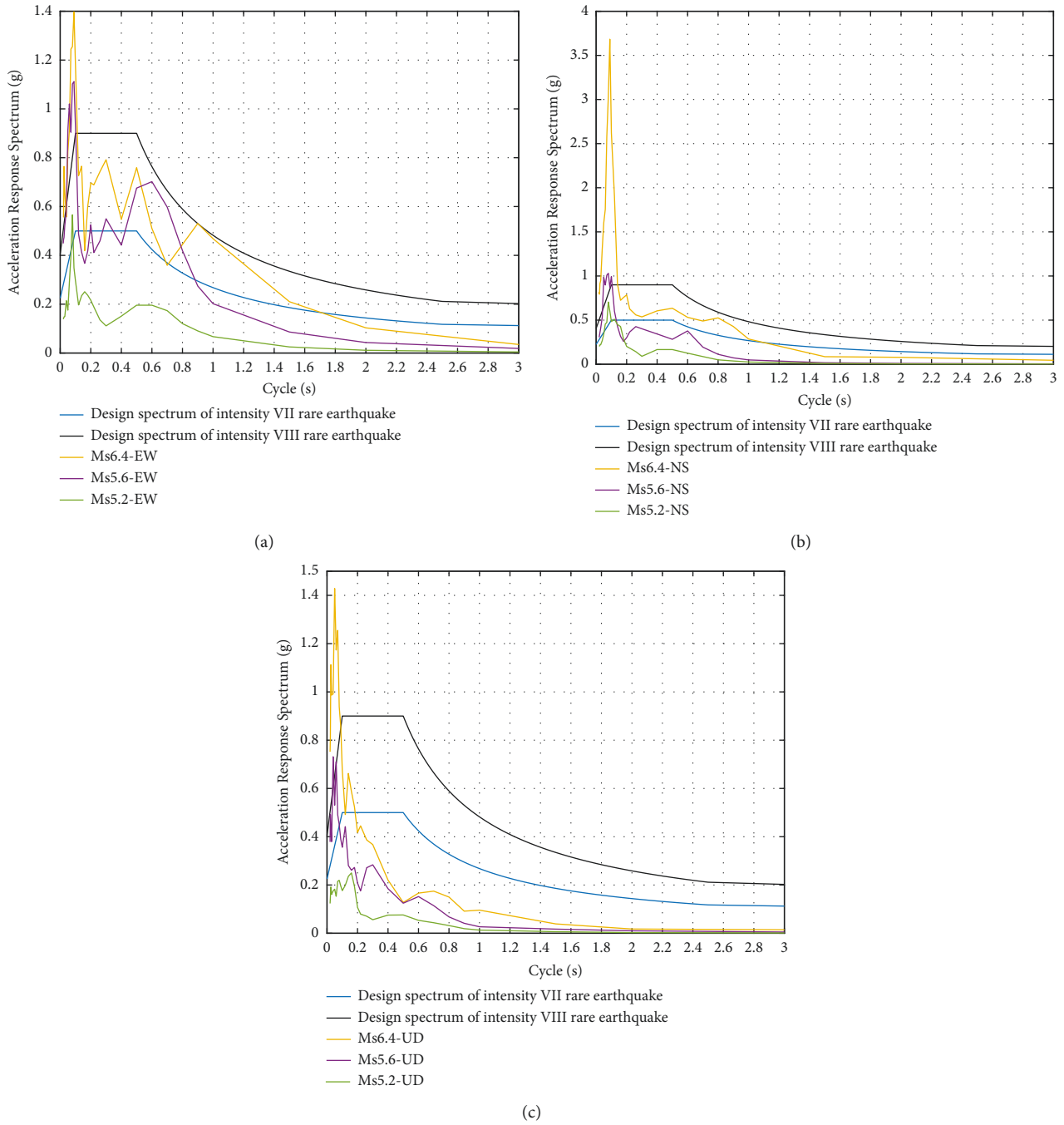

Figure 6: Comparison of acceleration response spectra (Sa) and code design spectra among the MS6.4, MS5.6, and MS5.2 earthquakes: (a) east-west; (b) north-south; and (c) vertical.

the main reinforcement of a pier is 28 mm, the diameter of the other reinforcement is 16 mm, the foundation is pile cap foundation, and the foundation conditions were added according to the geological survey data. The pier helps to ensure ductility and higher bearing capacity. Considering the E1 and E2 stages, the response of the pier of the bridge structure under the earthquake is studied and analysed [26].

5.2. Define the Constitutive Relationship of Reinforced Concrete. During the seismic analysis of the bridge, the $M - \varphi$ curve shall be defined according to the requirements of the specification. For the reinforced concrete pier, the concrete in the core area shall be calculated as constrained concrete [27], and the concrete within the thickness of the protective layer shall be calculated as unconstrained concrete. The corresponding ultimate compressive strain of concrete is calculated according to the Mander constitutive relationship, and the reinforcement and section data are imported. The hysteretic model of reinforcement constitutive relationship is based on the

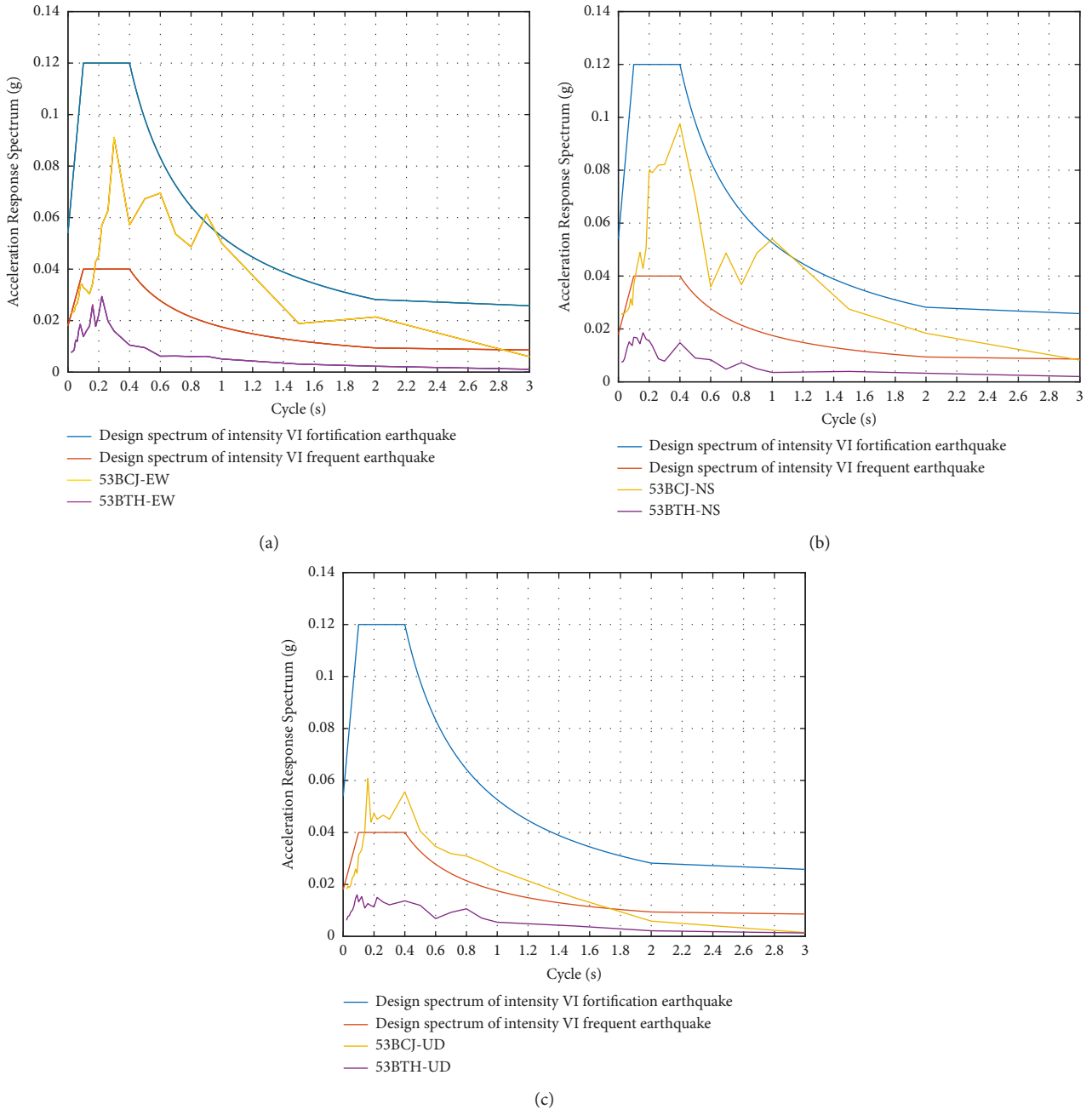

Figure 7: Comparison of acceleration response spectra (Sa) and code design spectra between a soil station (53BCJ) and a rock station (53BTH): (a) east-west; (b) north-south; and (c) vertical.

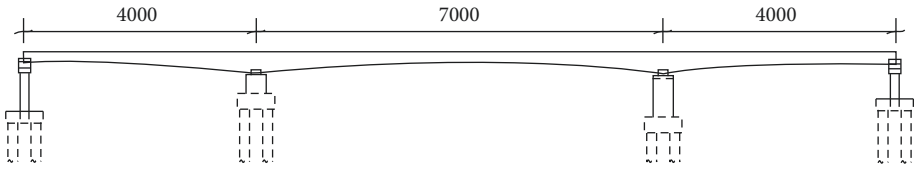

Figure 8: Bridge elevation.

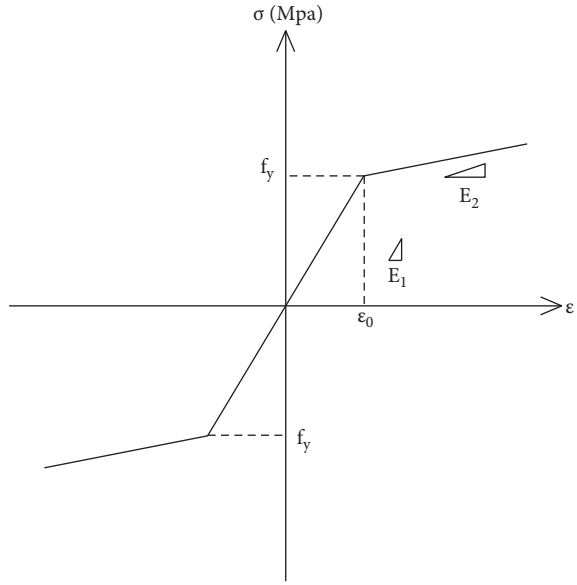

Figure 9: Constitutive relation of reinforcement.

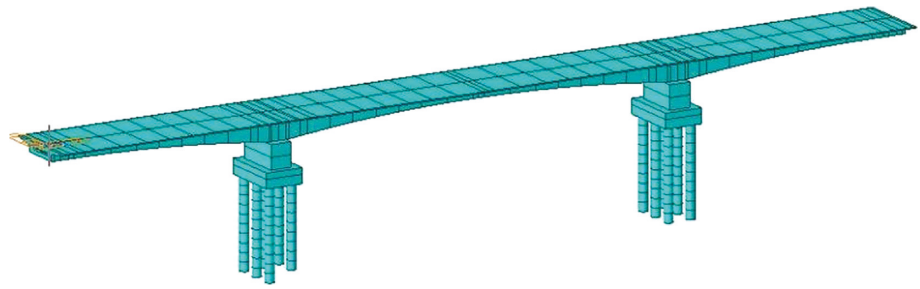

Figure 10: Finite element division of bridge elements.

double broken line model, in which Fy is 345 MPa, E1 is 210 Gpa, and E2 is 1% of E1 (Figure 9).

5.3. Finite Element Model and Modal Analysis. The dynamic calculation model of the bridge was established by Midas Civil software [28]. A total of 113 nodes were established for the whole bridge and divided into 96 units. The beam end and beam bottom were simplified as general support constraints [29], the superstructure and substructure were elastically connected, and the parts of the substructure were also elastically connected (Figure 10). The method was used to calculate the stiffness of the pile foundation in all directions. The structural load was converted into mass. The eigenvectors were computed using the Lanczos method, and the number of vibration modes was 110 [30]. The first 10 natural frequencies of the bridge structure and the cumulative participation mass of the first 110 modes were considered (Tables 2 and 3). The fundamental period of the bridge was 0.77 s, which is relatively small. The period basically changed in the first 5 modes. The cumulative participation mass of the first 67 modes exceeded 90% in the X and Y directions but did not exceed 90% in the Z direction until the 105th mode. The distribution of the three-dimensional cumulative participation rate of the first 110 modes is shown in Figure 11.

Table 2: First 10 natural frequencies and natural periods of the bridge structures.

Mode	Natural angular frequency (rad/sec)	Natural frequency (cycle/sec)	Natural period (sec)
1	8.213	1.307	0.765
2	8.737	1.391	0.719
3	11.445	1.822	0.549
4	14.957	2.380	0.420
5	15.356	2.444	0.409
6	17.089	2.720	0.368
7	20.840	3.317	0.301
8	25.400	4.043	0.247
9	34.298	5.459	0.183
10	40.157	6.391	0.156

5.4. Time History Conversion Response Spectrum. Consider that the time history analysis results are lower than the response spectrum results, to better reflect the impact of the earthquake on the bridge structures [31]. This study uses Midas Civil software to convert the three-dimensional

Table 3: Cumulative participation mass of the first 110 vibration modes of the bridge structures.

Mode	Vibration mode participation mass/ X (%)	Vibration mode participation mass/ Y (%)	Vibration mode participation mass/Z (%)
1	0	70.47	0
2	0	70.47	25.89
3	75.74	70.47	25.89
4	76.62	70.47	25.89
5	76.62	70.47	73.97
6	76.62	70.47	73.97
7	77.83	70.47	73.97
8	77.83	70.47	73.97
9	77.83	70.47	74.05
10	77.83	70.47	74.05
...	...	...	...
67	90.17	92.87	77.69
...	...	...	...
105	90.17	92.87	94.35

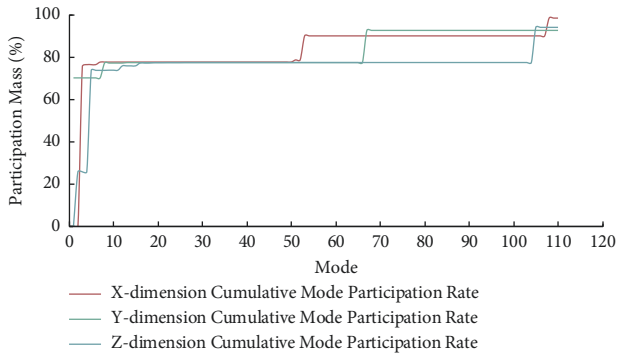

Figure 11: Three-dimensional cumulative mode participation rate.

seismic wave of the Ms6.4 earthquake at 53YBX into the response spectrum, hereinafter referred to as the converted response spectrum, and then compares the converted response spectrum with the displacement and internal force of the response spectrum under E1 and E2 in the Specifications for Seismic Design of Highway Bridges [32].

The seismic fortification intensity of the area where the earthquake was located (Yangbi Yi Autonomous County, Yunnan Province) is VIII, the Ci values are 0.5 and 1.7, respectively, under the seismic importance factors E1 and E2, the zoning characteristic period is 0.45 s, the PGA is 0.2 g, the bridge type is class B, the damping ratio is 0.05, and other relevant parameters were selected according to the Specifications for Seismic Design of Highway Bridges (2020). The response spectra are fitted (Figure 12).

Using the Midas Civil software, the maximum bending moment and displacement of the pier top and bottom of the bridge under E1 and E2 stages were solved according to the Specifications for Seismic Design of Highway Bridges, and the results were compared with the calculation results based on the time history seismic wave conversion response spectrum (Tables 4 and 5). The results show that the earthquake has little effect on the displacement of the bridge piers, which is much smaller than those at E1 and E2 stages.

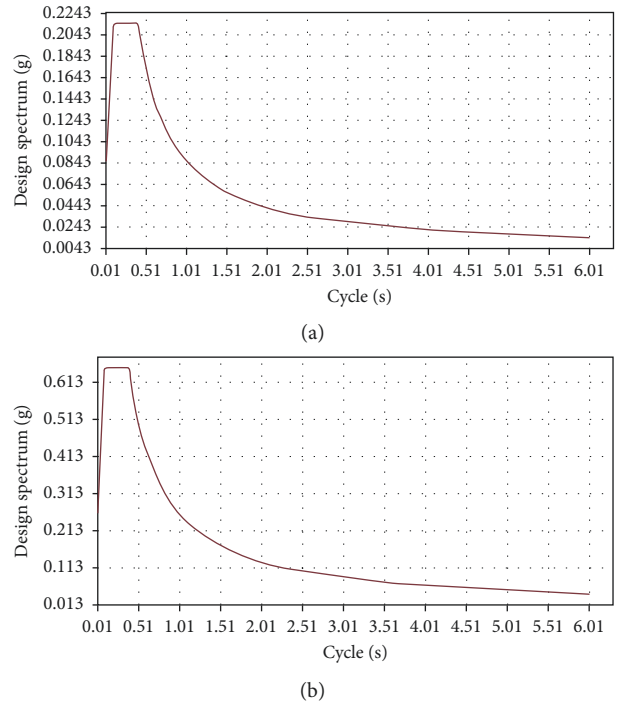

Figure 12: Three-dimensional cumulative mode participation rate: (a) E1 and (b) E2.

Table 4: Bending moment of pier (unit: kN m).

Pier	E1	E2	Conversion response spectrum
Pier top	53290.7	104141.3	56216.8
Pier bottom	30877.6	43904.3	48833.0

Table 5: Pier displacement (unit: mm).

Pier	E1	E2	Conversion response spectrum
Pier top	22.01	39.2	12.1
Pier bottom	17.8	33.7	10.4

The maximum bending moment generated at the top of the bridge piers exceeds the E1 design bending moment by 5.5%, which is 53.1% lower than the E2 design bending moment. The maximum bending moment generated at the bottom of the piers exceeds the E1 design bending moment by 58.2% and exceeds the E2 design bending moment by 11.2%, indicating that the earthquake had a greater impact on the bottom of the bridge piers and that the pier bottom might have entered the plastic stage. The specific checking calculation needs further investigation of the boundary constraints and pier reinforcement design.

6. Conclusion

The ground motion records obtained in Yangbi, Yunnan Province, on May 21, 2021, were processed by filtering and other conventional processing. The time-frequency analysis of ground motion signals was carried out using wavelet,

wavelet packet, and acceleration response spectra. A model was established to analyse the seismic response of a typical three-span continuous beam bridge, which provides important reference materials for the investigation of ground motion characteristics and engineering seismic damage in Southwest China. The following conclusions can be drawn:

(1) The maximum PGA of the Ms6.4 earthquake occurred at station 53YBX. The low-frequency signal energy is strong, and the energy is mainly concentrated in the 0–15 Hz range.

(2) With the increase in epicentral distance, the characteristic frequency bandwidth of an energy spectrum becomes narrower, the dominant energy is more concentrated in the low-frequency band, and the high-frequency energy decreases.

(3) The Sa value near the origin of the earthquake is relatively large. With an increase in magnitude of the earthquake, the Sa peak value rises and the long-period component becomes more significant; the site conditions tend to have a significant impact on ground motion and that soil field causes a more evident amplification effect on the acceleration response of ground surface than bedrock.

(4) This earthquake has little effect on pier displacement, which is far less than the design response spectrum of E1 and E2 stages. The maximum bending moment generated at the top of the pier is less than the E2 design bending moment, and the maximum bending moment generated at the bottom of the pier is greater than the E2 design bending moment, indicating that the earthquake has a greater impact on the bottom of the bridge pier, and the bottom of the pier may have entered the plastic stage.

Data Availability

Data for this study are provided by the Institute of Engineering Mechanics, China Earthquake Administration.

Conflicts of Interest

The authors declare that they have no conflicts of interest.

Acknowledgments

This research was funded by the Science for Earthquake Resilience, China Earthquake Administration (XH20058Y), and the "Qizhi" Talents Support Project of Lanzhou Institute of Technology (grant no. 2020QZ-05).

References

[1] F. Long, Y. P. Qi, and G. X. Yi, "Relocation of the Ms6.4 Yangbi earthquake sequence on May21,2021 in yunnan Province and its seismogenic structure analysis," *Chinese Journal of Geophysics*, vol. 64, no. 8, pp. 2631–2646, 2021.

[2] C. Y. Li, J. Y. Zhang, and W. Wang, "The seismogenic fault of the 2021 Yunnan Yangbi Ms6.4 earthquake," *Seismology and Geology*, vol. 43, no. 3, pp. 706–721, 2021.

[3] W. Wang, J. He, X. Wang et al., "Rupture process models of the Yangbi and Maduo earthquakes that struck the eastern Tibetan Plateau in May 2021," *Science Bulletin*, vol. 67, no. 5, pp. 466–469, 2022.

[4] B. Chen and H. J. Li, "Characteristics of strong ground motions during the May 21, 2021 M6.4 Yangbi, Yunnan earthquake," *Journal of Nanjing University of Technology (Natural Science Edition)*, vol. 37, no. 4, pp. 81–90, 2021.

[5] W. T. Tian, J. H. Dong, and B. Yang, "Basic characteristics of the three elements of strong ground motion of the Yangbi Ms6.4 earthquake inYun nan Province," *China Earthquake Engineering Journa*, vol. 63, no. 4, pp. 760–766, 2021.

[6] P. R. Beaudet, J. K. He, X. Wang, and Y. Zhou, "Synthesis of nonstationary seismic signals," *Bulletin of the Seismological Society of America*, vol. 60, no. 5, pp. 1615–1624, 1970.

[7] S. Mukherjee and V. K. Gupta, "Wavelet-based characterization of design ground motions," *Earthquake Engineering & Structural Dynamics*, vol. 31, no. 5, pp. 1173–1190, 2003.

[8] H. Y. Yu, D. Wang, and Y. Q. Yang, "The preliminary analysis of strong ground motion characteristics from the Ms8.0 wenchuan earthquake," *Earthquake Engineering and Engineering Dynamics*, vol. 29, no. 1, pp. 1–13, 2009.

[9] L. Hong and C. H. Li, "Wavelet transform and application in signal processing," *Machine Building and Automation*, vol. 41, no. 3, pp. 131–133, 2012.

[10] K. Gurley and A. Kareem, "Applications of wavelet transforms in earthquake, wind and ocean engineering," *Engineering Structures*, vol. 21, no. 2, pp. 149–167, 1999.

[11] J. Allen, "Short term spectral analysis, synthesis, and modification by discrete Fourier transform," *IEEE Transactions on Acoustics, Speech, & Signal Processing*, vol. 25, no. 3, pp. 235–238, 1977.

[12] J. Morlet, G. Arens, E. Fourgeau, and D. Glard, "Wave propagation and sampling theory-Part I: complex signal and scattering in multilayered media," *Geophysics*, vol. 47, no. 2, pp. 203–221, 1982.

[13] M. Stephane, *A Wavelet Tour of Signal Processing*, Elsevier, Pittsburgh, 1999.

[14] D. F. Zhao, G. Y. Chen, and S. Chen, "Analysis of time-frequency characteristics of shaking table test data of subway underground station structure with different stiffness," *Journal of Nanjing University of Technology (Natural Science Edition)*, vol. 37, no. 4, pp. 77–84, 2015.

[15] M. P. Fargues, H. F. Overdyk, R. Wang, and Y. Zhou, "Wavelet-based detection of frequency hopping signals," in *Proceedings of the Conference Record of the Thirty-First Asilomar Conference on Signals, Systems and Computers (Cat. No.97CB36136)*, no. 1, pp. 515–519, Pacific Grove, CA, USA, November 1997.

[16] S. P. Wang, W. G. Zhang, and G. Y. Zhang, "Identification of structural parameters from free vibration data using Gabor wavelet transform," *Mechanical Systems and Signal Processing*, vol. 147, no. 2, pp. 107–114, 2020.

[17] X. Jin, L. C. Kang, and Y. P. Ou, "Acceleration spectrum attenuation relation for small and moderate earthquakes in Fujian region," *J Earthquake Engineering and Engineering Dynamics*, vol. 29, no. 5, pp. 52–58, 2009.

[18] N. C. Nigam and P. C. Jennings, "Calculation of response spectra from strong-motion earthquake records," *Bulletin of the Seismological Society of America*, vol. 59, no. 2, pp. 909–922, 1969.

[19] B. Mohraz, "A study of earthquake response spectra for different geological conditions," *Bulletin of the Seismological Society of America*, vol. 66, no. 3, pp. 915–935, 1976.

[20] P. K. Malhotra, "Smooth spectra of horizontal and vertical ground motions," *Bulletin of the Seismological Society of America*, vol. 96, no. 2, pp. 506–518, 2006.

[21] E. Kuribayashi, T. Iwasaki, Y. Iida, and K. Tuji, "Effects of seismic and subsoil conditions on earthquake response spectra," *International conference on microzonation for safer construction research and application*, vol. 2, pp. 668–671, 1972.

[22] Q. Han, X. Du, J. Liu, Z. Li, L. Li, and J. Zhao, "Seismic damage of highway bridges during the 2008 Wenchuan earthquake," *Earthquake Engineering and Engineering Vibration*, vol. 8, no. 2, pp. 263–273, 2009.

[23] F. X. Ding, W. Xia, x. Ping, and W. Y. Zhi, "New damage ratio strength criterion for concrete and lightweight aggregate concrete," *ACI Structural Journal*, vol. 118, no. 6, pp. 165–178, 2021.

[24] H. A. Mohamed, M. M. Husain, and A. M. Aboraya, "Progressive collapse of RC box girder bridges due to seismic actions," *Advances in Civil Engineering*, vol. 2020, no. 2, Article ID 1919683, 17 pages, 2020.

[25] S. Talatahari, V. P. Singh, A. H. Alavi, and F. Kang, "Soft computing methods in civil engineering," *The Scientific World Journal*, vol. 2015, no. 1, Article ID 605871, 2 pages, 2015.

[26] J. Deng, T. Liu, W. Xie, and W. Lu, "Study on repaired earthquake-damaged bridge piers under seismic load," *Advances in Materials Science and Engineering*, vol. 2015, Article ID 295392, 10 pages, 2015.

[27] W. G. Corley, "Applicability of seismic design in mitigating progressive collapse," in *Proceedings of the National Workshop on Prevention of Progressive Collapse*, p. 13, Rosemont, IL, USA, July 2002.

[28] H. Wibowo, S. S. Reshotkina, and D. T. Lau, N. L. St John's, Modeling progressive collapse of RC bridges during earthquakes," in *Proceedings of the CSCE Annual General Conference 2009: On the Leading Edge*, p. 11, Canada, May 2009.

[29] C. Akogul and O. Celik, "Effect of elastomeric bearing modeling parameters on the seismic design of RC highway bridges with precast concrete girders," in *Proceedings of the 14th World Conference on Earthquake Engineering (14WCEE)*, Beijing, China, October 2008.

[30] A. Chopra, *Dynamics of Structures: Aeory and Applications to Earthquake Engineering*, Prentice-Hall, Englewood Cliffs, NJ, USA, 1995.

[31] Z. Sun, D. Wang, X. Du, and B. Si, "Rapid repair of severely earthquake-damaged bridge piers with flexural-shear failure mode," *Earthquake Engineering and Engineering Vibration*, vol. 10, no. 4, pp. 553–567, 2011.

[32] N. Shome, C. A. Cornell, P. Bazzurro, and J. E. Carballo, "Earthquakes, records, and nonlinear responses," *Earthquake Spectra*, vol. 14, no. 3, pp. 469–500, 1998.